Nanoscale

PAPER

View Article Online
View Journal | View Issue

Cite this: *Nanoscale*, 2016, **8**, 8583

Fluoride-induced modulation of ionic transport in asymmetric nanopores functionalized with "caged" fluorescein moieties

Mubarak Ali,*[a,b] Ishtiaq Ahmed,[c] Patricio Ramirez,[d] Saima Nasir,[a] Javier Cervera,[e] Christof M. Niemeyer[c] and Wolfgang Ensinger[a]

Received 12th January 2016,
Accepted 18th March 2016

DOI: 10.1039/c6nr00292g

www.rsc.org/nanoscale

We demonstrate experimentally and theoretically a nanofluidic fluoride sensing device based on a single conical pore functionalized with "caged" fluorescein moieties. The nanopore functionalization is based on an amine-terminated fluorescein whose phenolic hydroxyl groups are protected with *tert*-butyldiphenylsilyl (TBDPS) moieties. The protected fluorescein (Fcn-TBDPS–NH_2) molecules are then immobilized on the nanopore surface *via* carbodiimide coupling chemistry. Exposure to fluoride ions removes the uncharged TBDPS moieties due to the fluoride-promoted cleavage of the silicon–oxygen bond, leading to the generation of negatively charged groups on the fluorescein moieties immobilized onto the pore surface. The asymmetrical distribution of these groups along the conical nanopore leads to the electrical rectification observed in the current–voltage (*I*–*V*) curve. On the contrary, other halides and anions are not able to induce any significant ionic rectification in the asymmetric pore. In each case, the success of the chemical functionalization and deprotection reactions is monitored through the changes observed in the *I*–*V* curves before and after the specified reaction step. The theoretical results based on the Nernst–Planck and Poisson equations further demonstrate the validity of an experimental approach to fluoride-induced modulation of nanopore current rectification behaviour.

Introduction

Over the recent years, the community working on host–guest and supramolecular chemistry has paid much attention to miniaturize anion sensing devices.[1] Anions play a fundamental role in a variety of chemical and biological processes. In particular, fluoride is considered a small, highly electronegative ion with hard Lewis basic nature. In living organisms, fluoride plays a pivotal role in cell signaling transductions and also induces apoptosis.[2] A deficiency or excess of fluoride beyond the optimum limit can cause various diseases in human beings.[3] For example, fluoride deficiency can adversely affect human development and lead to dental caries and osteoporosis.[4] On the contrary, excessive ingestion of fluoride can cause various ailments in humans such as dental and skeletal fluorosis, nephrotoxic changes and urolithiasis.[5]

To date, different fluorescent and colorimetric chemosensors have been designed for the sensing of fluoride anions.[1c,4b,6] The sensing principle mainly relies on the Lewis acid–base interactions, metal ion displacement from the metallic complexes and fluoride-induced desilylation reaction. While most of the reported chemosensors can detect fluoride with high sensitivity and specificity, the majority of them are functional only in organic solvents or mixed organic–water solutions, which limits their use in biological applications. Hence, the design and development of a sensing nanodevice that selectively detects fluoride under aqueous physiological conditions is still challenging.

Ion channels and pores regulate the flow of ions across the membrane, facilitating the chemical and electrical communication with the extracellular environment in living organisms.[7] The protein ion channels are precisely controlled structures with defined interfacial chemistry which have been proved to be useful for a variety of applications in nanobiotechnology such as sensing and manipulation of single molecules.[8] However, the fragility and sensitivity of the embedding lipid bilayers restrain their suitability in practical cases. Conversely, synthetic nanopores fabricated in solid-state and polymeric

[a]*Technische Universität Darmstadt, Fachgebiet Materialanalytik, Alarich-Weiss-Str. 2, D-64287 Darmstadt, Germany. E-mail: m.ali@ca.tu-darmstadt.de*
[b]*Matrialforschung, GSI Helmholtzzentrum für Schwerionenforschung, Planckstr. 1, D-64291 Darmstadt, Germany. E-mail: m.ali@gsi.de*
[c]*Karlsruhe Institute of Technology (KIT), Institute for Biological Interfaces (IBG-1), Hermann-von-Helmholtz-Platz, D-76344 Eggenstein-Leopoldshafen, Germany*
[d]*Departament de Física Aplicada, Universitat Politécnica de València, E-46022 València, Spain*
[e]*Departament de Física de la Terra i Termodinàmica, Universitat de València, E-46100 Burjassot, Spain*

materials have recently attracted interest because their shape, size, and surface properties can be tuned on demand.[9] Moreover, they exhibit more chemical and mechanical robustness compared with their biological counterparts. To broaden the scope and application of nanoporous systems, a variety of responsive molecules and functional groups have been immobilized onto the inner pore walls.[10] Upon exposure to a specific analyte or an external stimulus, the modified pores undergo changes in their effective diameters and surface charge polarity, resulting in the variation of ionic flux across the membrane. Thus, nanofluidic sensing devices based on nanopores have been employed for the detection of a variety of analyte molecules.[11]

We demonstrate here a nanofluidic fluoride sensing device based on a single asymmetric pore functionalized with "caged" fluorescein moieties. To this end, we have synthesized an amine-terminated fluorescein whose phenolic hydroxyl groups are protected with *tert*-butyldiphenylsilyl (TBDPS) moieties. The protected fluorescein (Fcn-TBDPS–NH_2) molecules are then immobilized on the pore surface *via* carbodiimide coupling chemistry. On exposure to fluoride ions, the uncharged TBDPS moieties are removed due to the fluoride-promoted cleavage of the silicon–oxygen bond, leading to the generation of negatively charged functionalities on the pore surface. This fact leads to the permselective transport of ions through the nanopore. On the contrary, other halides and anions do not induce any significant change in the rectified ion flux across the asymmetric pore. The success of the chemical functionalization and deprotection reactions is monitored through the changes in electrical current–voltage (*I*–*V*) curves before and after the specified reaction step.

Experimental

Materials

The irradiation of 12 μm thick polymer membranes of polyethylene terephthalate (PET) (Hostaphan RN 12, Hoechst) was performed at the GSI Helmholtz Centre for Heavy Ion Research (GSI, Darmstadt) with Au ions (energy: 11.4 MeV per nucleon, ion fluence: either single or 10^7 ions per cm^2).

All the chemicals and solvents such as *N*-(3-dimethylaminopropyl)-*N'*-ethylcarbodiimide hydrochloride (EDC-HCl), pentafluorophenol (PFP), 5(6)-carboxyfluorescein (Fcn), *N*-Boc-1,6-hexanediamine, *N*,*N*-diisopropylethylamine (DIPEA), *tert*-butylchlorodiphenylsilane (TBDPSCl), trifluoroacetic acid (TFA), hydroxybenzotriazole (HOBt), tetrabutylammoniumfluoride (TBAF), tetrabutylammonium chloride (TBACl), tetrabutylammonium bromide (TBABr), tetrabutylammonium iodide (TBAI), disodium hydrogen phosphate (Na_2HPO_4), sodium nitrate ($NaNO_3$), sodium bicarbonate ($NaHCO_3$), sodium acetate (CH_3COONa), sodium sulphate (Na_2SO_4), sodium fluoride (NaF), sodium chloride (NaCl), sodium bromide (NaBr) and sodium iodide (NaI) were purchased from Sigma-Aldrich, Taufkirchen, Germany, and used without further purification.

^1H and ^{13}C NMR spectra were recorded at 500 and 125 MHz in $CDCl_3$, respectively. High-resolution mass spectra were measured using a Finnigan MAT90 mass spectrometer. Analytical TLC (silica gel, 60F-54, Merck) and spots were visualized under UV light and/or phosphomolybdic acid–ethanol. Flash column chromatography was performed with silica gel 60 (70–230 mesh, Merck) and basic aluminum oxide (activated, basic, ~150 mesh, 58 Å, Aldrich).

Fabrication of the conical nanopore

Before chemical etching, the ion tracked PET membranes were further irradiated with UV light from each side for 30 min in order to sensitize the latent tracks. These tracks were converted into conical nanopores by the asymmetric track-etching technique reported by Apel and co-workers.[12] For this purpose, a custom-made conductivity cell with three compartments was employed for the fabrication of single-pore and multipore membranes at the same time. A single-shot membrane and a membrane irradiated with 10^7 ions per cm^2 were placed on both sides of the middle chamber of the conductivity cell and clamped tightly. The middle compartment had apertures on both sides and was filled with an etching solution (9 M NaOH). The other two compartments on either side of the middle one were filled with an acidic stopping solution (1 M KCl + 1 M HCOOH). The gold electrodes were placed on both sides of the single-ion irradiated membrane and a potential (−1 V) was applied across the membrane to monitor the etching process carried out at room temperature. During this process, the current remained zero as long as the pore was not yet etched through. After the breakthrough, a point at which the etchant penetrated across the whole length of the membrane, an increase in the ionic current flowing through the nascent pore was observed. The etching process was terminated when the current reached a certain value. Immediately after etching, the membranes were thoroughly washed with the stopping solution in order to neutralize the etchant, followed by washing with deionized water. The etched membranes were then dipped in deionized water overnight in order to remove the residual salts.

Synthesis of amine-terminated "caged" fluorescein (4)

Synthesis of compound (2). The compound (2) in Fig. 1A was synthesized by a carbodiimide coupling reaction with a slight modification of the reported method.[13] To a stirred solution of 5(6)-carboxyfluorescein (**1**) (500 mg, 1.32 mmol) in anhydrous DMF (10 mL), EDC–HCl (300 mg, 1.6 mmol) and HOBt (244 mg, 1.6 mmol) were added. The resulting mixture was stirred at room temperature for 20 min. Then *N*-Boc-1,6-hexanediamine (0.36 mL, 1.62 mmol) was added followed by *N*,*N*-diisopropylethylamine (DIPEA) (0.7 mL, 4.0 mmol). The reaction mixture was further allowed to stir at room temperature overnight. Solvent evaporation under reduced pressure gave a brown residue which was purified by silica gel column chromatography eluting with pure dichloromethane, increasing to 10% methanol and 1% CH_3COOH in dichloromethane,

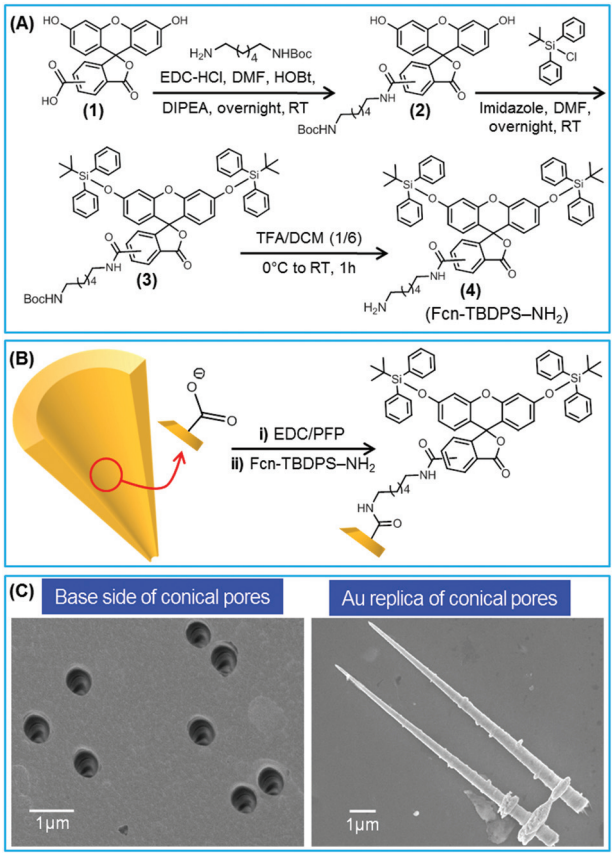

Fig. 1 (A) Synthesis of "caged" aminofluorescein (Fcn-TBDPS–NH_2): (B) the functionalization of the carboxylic acid groups on the surface of the asymmetric nanopore with amine-terminated fluorescein (Fcn-TBDPS–NH_2) moieties *via* carbodiimide coupling chemistry. (C) FESEM images of asymmetrically etched membranes containing 10^7 pore per cm^2 from the base side and Au replica deposited inside the conical nanopores.

afforded the fluorescein derivative **2** as a thick yellow oil (587 mg, 77%).

^{1}H NMR (500 MHz, CD_3OD, mixture of isomers): δ 1.23–1.28 (m, 4H), 1.32–1.37 (m, 4H), 1.39 (s, 9H), 1.40 (s, 9H), 1.44–1.50 (m, 4H), 1.60–1.65 (m, 4H), 2.97 (t, J = 6.9 Hz, 2H), 3.03 (t, J = 6.9 Hz, 2H), 6.51–6.56 (m, 4H), 6.58–6.63 (m, 4H), 6.70–6.74 (m, 4H), 7.28 (d, J = 8.2 Hz, 1H), 7.39–7.48 (m, 2H), 7.66 (s, 1H), 7.72 (d, J = 8.2 Hz, 1H), 7.81 (d, J = 8.2 Hz, 1H), 7.94 (s, 1H), 8.05 (d, J = 8.2 Hz, 1H), 8.12 (dd, J = 1.69, 8.2 Hz, 1H), 8.20 (dd, J = 1.69, 8.2 Hz, 1H), 8.44 (br s, 1H).

^{13}C NMR (125 MHz, CD_3OD, mixture of isomers): δ 29.9, 30.1, 30.2, 30.3, 31.5, 32.7, 32.9, 33.4, 34.4, 39.7, 43.7, 43.8, 61.0, 78.1, 82.4, 106.3, 114.3, 116.4, 120.9, 126.6, 127.5, 128.3, 128.8, 130.0, 130.7, 131.1, 132.1, 132.7, 132.8, 138.1, 140.4, 144.9, 156.6, 156.9, 158.9, 161.0, 161.1, 163.9, 164.0, 167.4, 170.5, 170.8, 173.2.

HRMS-FAB: calcd for $C_{32}H_{34}N_2O_8$ $[M + H]^+$ 575.2391, found $[M + H]^+$ 575.2388.

Synthesis of compound 3. The hydroxyl groups on the fluorescein derivative (**2**) were protected with *tert*-butylchlorodiphenylsilane (TBDPSCl) *via* a silylation reaction.[14] To a solution of compound (**2**) (300 mg, 0.52 mmol) in anhydrous DMF (10 ml), imidazole (177 mg, 2.61 mmol) was added. The mixture was stirred under a nitrogen atmosphere at room temperature. After 15 min, TBDPSCl (0.55 mL, 2.09 mmol) was added dropwise. The reaction mixture was allowed to stir at room temperature overnight. The solvent was evaporated under reduced pressure to give a yellow residue which was purified by silica gel column chromatography eluting with pure dichloromethane, increasing to 2% methanol in dichloromethane to afford the TBDPS boc-protected fluorescein derivative (**3**) as a yellow oil (466 mg, 85%).

^{1}H NMR (500 MHz, $CDCl_3$, mixture of isomers): δ 1.01–1.21 (m, 36H), 1.32–1.38 (m, 4H), 1.41–1.43 (s, 18H), 1.43–1.50 (m, 4H), 1.53–1.66 (m, 4H), 1.60–1.65 (m, 4H), 3.12 (t, J = 6.9 Hz, 2H), 3.38–3.48 (m, 4H), 6.35–6.46 (m, 7H) 6.57–6.65 (m, 3H), 7.34–7.41 (m, 16H), 7.40–7.45 (m, 8H), 7.66–7.72 (m, 14H), 8.17–8.20 (m, 1H), 8.34 (br s, 1H).

^{13}C NMR (125 MHz, $CDCl_3$, mixture of isomers): δ 26.4, 28.4, 30.0, 31.4, 39.7, 39.9, 79.0, 83.5, 107.4, 107.5, 111.1, 116.2, 127.6, 127.9, 128, 6, 128.7, 129.4, 130.1, 132.1, 134.8, 135.3, 136.7, 141.0, 152.0, 153.2, 155.2, 156.2, 157.4, 157.5, 165.7, 168.7.

HRMS-FAB: calcd for $C_{64}H_{71}N_2O_8Si_2$ $[M + H]^+$ 1051.4744, found $[M + H]^+$ 1051.4742.

Synthesis of compound (4). Trifluoroacetic acid (TFA) (2 mL) was added into a solution of compound (**3**) (100 mg) in dichloromethane (12 mL) at 0 °C. The reaction mixture was stirred at room temperature until TLC showed completion of the reaction (1–2 h). Then dichloromethane (10 mL) was added and the solvent was evaporated under reduced pressure. In order to remove the traces of TFA, the residue was further co-evaporated with dichloromethane (3 × 15 mL) and toluene (1 × 10 mL) to obtain TBDPS protected free amino terminated fluorescein (**4**) as a thick yellow oil (82 mg, 91%).

^{1}H NMR (500 MHz, CD_3OD, mixture of isomers): δ 1.02–1.04 (m, 42H), 1.08–1.12 (m, 4H), 1.61–1.24 (m, 6H), 1.41–1.53 (m, 8H), 1.60–1.76 (m, 8H), 2.89–2.96 (m, 4H), 3.37 (t, J = 7.1 Hz, 2H), 3.49 (t, J = 7.1 Hz, 2H), 3.60–3.66 (m, 2H), 3.71–3.78 (m, 2H), 6.82–6.86 (m, 3H), 6.97–7.02 (m, 6H), 7.35–7.44 (m, 28H), 7.67–7.70 (m, 6H), 7.73–7.75 (m, 14H), 8.20–8.28 (m, 2H).

^{13}C NMR (125 MHz, CD_3OD, mixture of isomers): δ 25.8, 27.0, 27.1, 28.7, 28.8, 30.2, 39.2, 39.5, 83.1, 102.1, 112.0, 113.5, 114.3, 114.9, 115.7, 116.6, 118.9, 127.1, 127.4, 129.0, 129.4, 133.2, 134.5, 135.1, 135.8, 158.6, 158.9, 159.2, 159.5, 166.6, 166.8.

HRMS-FAB: calcd for $C_{59}H_{63}N_2O_6Si_2$ $[M + H]^+$ 951.4146, found $[M + H]^+$ 951.4147.

Chemical functionalization of the nanopore

The carboxyl groups exposed on the pore surface were first converted into amine-reactive esters through carbodiimide coupling chemistry. To this end, the track-etched single-pore membrane was immersed in an ethanol solution containing EDC (100 mM) and PFP (200 mM) at room temperature. The activation process was carried out for 1 h. The activated

membrane was washed with ethanol several times. Then, the activated pore was dipped in Fcn-TBDPS–NH_2 (10 mM) solution prepared in anhydrous ethanol for 15 h. During this reaction period, amine-reactive PFP-esters were covalently coupled with the terminal amine group of the "caged" fluorescein. Subsequently, the modified pore was washed thoroughly with ethanol followed by careful rinsing with deionized water.

Current–voltage measurements

The unmodified and modified pores were characterized by measuring the current–voltage (*I–V*) curves before and after functionalization. To this end, the single-pore membrane was fixed between the two halves of the conductivity cell. An electrolyte (0.1 M KCl) prepared in 10 mM tris-buffer (pH 7.6), was filled on both sides of the membrane. An Ag/AgCl electrode was placed in each half-cell solution and the ionic current flowing through the single pore membrane was measured with a picoammeter/voltage source (Keithley 6487, Keithley Instruments, Cleveland, OH). The ground electrode was placed on the base opening side of the asymmetric pore and the *I–V* curves were recorded by applying a scanning triangle voltage signal from +2 to −2 V across the membrane.

The 1 mM solutions of various anions (TBA^+ and Na^+ salts) were prepared in a 0.1 M KCl solution with 10 mM tris-buffer (pH 7.6) and the corresponding *I–V* curves were recorded under symmetric electrolyte conditions.

Results and discussion

The reaction scheme for the synthesis of "caged" aminofluorescein (Fcn-TBDPS–NH_2) is shown in Fig. 1A. First, the fluorescein derivate (**2**) was synthesized by covalent coupling of commercially available 5(6)-carboxyfluorescein (**1**) and *N*-Boc-1,6-hexanediamine performed in the presence of EDC, HOBt and DIPEA in anhydrous DMF overnight. Then, the protection of the phenolic hydroxyl groups was achieved through the silylation reaction using imidazole and TBDPSCl in dried DMF, resulting in the TBDPS-protected fluorescein derivate (**3**). Subsequently, deprotection of *N*-Boc groups was achieved by using trifluoroacetic acid (TFA) in dichloromethane (DCM) to afford TBDPS-protected aminofluorescein (**4**). The chemical structures of fluorescein derivatives were characterized by ^1H NMR, ^{13}C NMR and HRMS-FAB techniques.

Single asymmetric nanopores were fabricated in 12 μm thick polyethylene terephthalate (PET) membranes irradiated with swift heavy ions by the well-established asymmetric track-etching technique.[12] The asymmetric nanopores contain tip openings and base openings on the side of the membrane facing stopping and etching solutions, respectively (Fig. 1C). Due to chemical etching of the ion tracks, carboxylic acid (–COOH) groups are generated on the pore surface. These groups are employed to modulate the pore surface chemical properties through amide coupling of amine-terminated molecules.

Fig. 1B shows the covalent attachment of Fcn-TBDPS–NH_2 molecules onto the pore surface. First, the carboxylic acid groups on the pore surface were activated by exposing the single-pore membrane to an ethanolic solution of EDC and pentafluorophenol (PFP), resulting in the formation of an amine-reactive PFP reactive-ester on the pore walls. Subsequently, the PFP-reactive intermediate was covalently attached to the terminal-amine group of the Fcn-TBDPS–NH_2 molecules.

To demonstrate the success of chemical functionalization, the *I–V* curves of the single nanopore were measured before and after modification. The membrane was assembled between the two chambers of the conductivity cell. The electrolyte (0.1 M KCl) solution prepared in tris-buffer (10 mM, pH 7.6) was filled on both sides of the conical nanopore and the electrodes on each side of the nanopore were arranged in such a way that high currents at positive voltages and low currents at negative voltages were obtained. Fig. 2 shows the resulting *I–V* curves before and after the attachment of "caged" fluorescein moieties. Previous experimental[10,11] and theoretical[15] studies have proved that the as-prepared single conical nanopores exhibit cation-selectivity and rectify the ion current (*i.e.*, cations preferentially flow from the tip towards the base opening) due to the presence of ionized $-COO^-$ groups on the pore surface. When a potential is applied across the membrane, the current rectification is a consequence of the combined effects of geometry and electrostatic asymmetries. As expected, immobilization of "caged" fluorescein resulted in the loss of the pore surface charge due to the presence of uncharged TBDPS moieties. Eventually, the modified pore behaved like an ohmic resistor as evidenced from the *I–V* curve. Moreover, the rectification degree (f_{rec}) of the conical

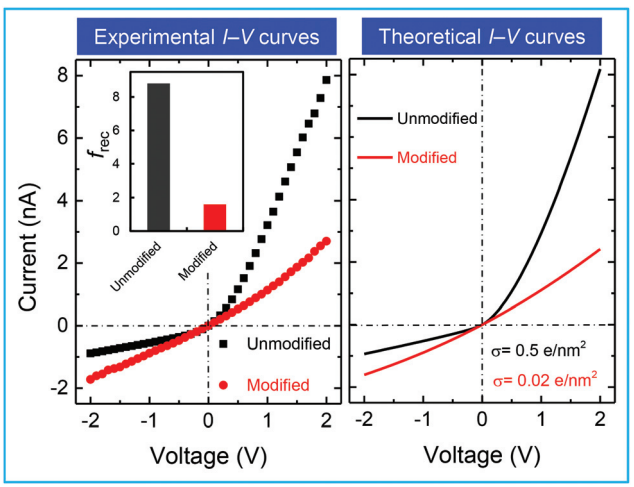

Fig. 2 Experimental and theoretical *I–V* characteristics of the single conical pore before (black) and after (red) the immobilization of "caged" fluorescein moieties. The experimental *I–V* curves are recorded in 0.1 M KCl (tris-buffer, pH 7.6) solution. The radii of the small and large pore openings are a_L = 10 and a_R = 250 nm, respectively. The inset shows the rectification ratios (f_{rec}) before and after pore modification. The error bars of the experimental data are smaller than the symbol size.

nanopore is directly related to the magnitude of the surface charges. In this case, f_{rec} is obtained from the ratio of positive and negative currents at 2 V. After the pore modification, f_{rec} decreases from ~ 8.8 to 1.6, further confirming the successful anchoring of "cage" fluorescein chains on the pore surface. The theoretical curves of Fig. 2 were calculated using a continuous Poisson–Nernst–Planck (PNP) model previously developed, which allows for the calculation of the ionic fluxes at a given applied voltage. The model parameters to be determined are the radii of the small and large pore openings, a_L and a_R, respectively, and the surface concentration of fixed charges on the pore wall, σ. The radius of the large opening was obtained by AFM techniques using a membrane multipore sample etched at the same time as the single pore sample employed in the experiments (Fig. 1C). The radius of the small opening was calculated from the *I–V* curve of the unmodified pore measured at 1 M KCl concentration and small voltages. Under these conditions, the mobile charges screen the fixed charge groups ($\sigma = 0$) and the *I–V* curve is approximately linear. The results obtained using this approach were $a_L = 10$ nm and $a_R = 250$ nm. Once the pore radii were obtained, the only remaining model parameter σ was calculated by fitting the experimental curves to the theory. In the case of the single conical pore of Fig. 2, the surface charges obtained were $\sigma = 0.5$ e nm^{-2} and $\sigma = 0.02$ e nm^{-2} before and after the immobilization of "caged" fluorescein moieties, respectively, where e is the elementary charge.

After functionalization, we proceeded to study the fluoride-promoted cleavage of *tert*-butyldiphenylsilyl (TBDPS) moieties on the "caged" fluorescein chains immobilized on the pore surface. In the previously reported fluoride sensing systems, TBDPS groups have been employed for the protection of hydroxyl-containing compounds which can be easily and irreversibly removed with fluoride ions.[5a,16] The deprotection of TBDPS was achieved through the formation of the Si–F bond (TBDPS–F) at the expense of the Si–O bond cleavage because of the unique interaction between the Lewis base (fluoride) and acid (silicon center). Keeping in mind the selective fluoride-induced cleavage of the Si–O bond, the modified nanopore was exposed to an electrolyte solution containing various halides (tetrabutylammonium salt, TBA^+) including fluoride (F^-), chloride (Cl^-), bromide (Br^-) and iodide (I^-), separately. Fig. 3B shows the *I–V* characteristics of the modified pore before and after exposure to halide solutions. For the Cl^-, Br^- and I^- ions, we did not observe any significant change in the *I–V* curves as shown in Fig. 3B, even at a high concentration (1 mM). On the contrary, upon exposure to even lower F^- concentrations, the pore exhibits high ionic current rectification (Fig. 3C). It is known that fluoride anions selectively break the Si–O bonds and then the uncharged TBDPS moieties are detached from the pore surface. This resulted in the generation of phenolic (–PhOH) and carboxylic (–COOH) acid functionalities on the fluorescein moieties. Under our experimental conditions, the exposed phenolate ($-PhO^-$) and carboxylate ($-COO^-$) groups impart a negative charge to the pore walls, resulting in current rectification because of the selective transport of cations. This fact shows that on exposure to fluoride, the inner pore was switched from a hydrophobic and uncharged non-conductive state to a hydrophilic and charged conductive state. Thus, the fluoride-induced changes in the surface polarity modulate the permselective behavior of the pore.

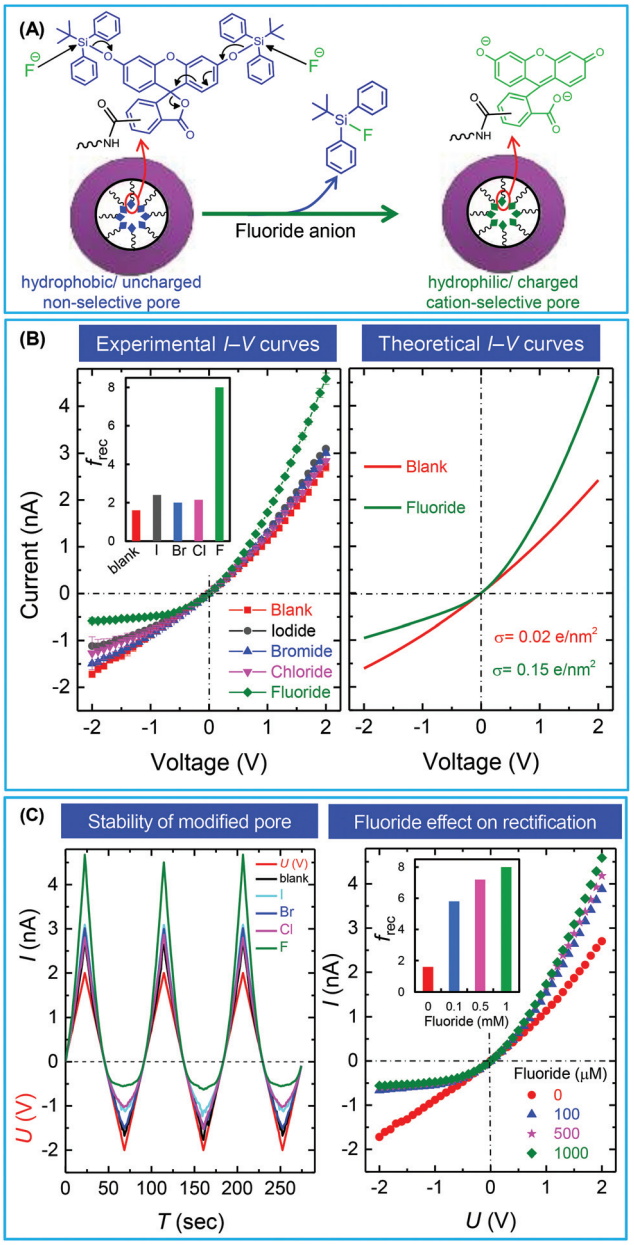

Fig. 3 (A) Scheme representing the removal of *tert*-butyldiphenylsilyl groups through fluoride-promoted cleavage of the Si–O bond. (B) Experimental and theoretical *I–V* characteristics of the modified pore before (blank) and after the addition of various halide anions (1 mM, TBA^+ salts) into the electrolyte solution, separately. (C) Measurement cycles for the stability of the modified pore obtained from the applied voltage and current signals corresponding to the experimental *I–V* curves shown in (B). *I–V* characteristics of the modified pore exposed to various concentrations of fluoride anions. The inset shows the rectification ratio (f_{rec}) on exposure to halide anion solutions.

Fig. 3C shows the stability of the modified pore and the effect of fluoride anion concentration on current rectification. The functionalized pore exhibits approximately stable current signals over triangular voltage sweeps. Before exposure to 1 mM solution of TBAF, we have also measured the *I–V* characteristics of the modified pore in the presence of various fluoride concentrations in the electrolyte solution. For the case of 0.1, 0.5 and 1 mM concentrations, the rectification ratio f_{rec} obtained from their corresponding *I–V* curve was increased from 1.6 to 5.8, 7.1 and 8.0, respectively. This fact indicated the effective cleavage of uncharged TBDPS moieties and the concomitant increase in the pore surface charge polarity. The theoretical curves of Fig. 3B show an increase in the pore surface charge (σ) from 0.02 to 0.15 e nm^{-2} after the fluoride mediated desilylation reaction.

After the desilylation, the next step was to tune the nanopore transport properties under physiological conditions. Previous studies have demonstrated that the fluorescein molecule under aqueous conditions may exist in cationic, neutral and anionic forms depending on the solution pH.[17] Under acidic conditions (pH 5.5), the fluorescein on the pore surface occurred in the form of lactonic/quinonoid moieties with net charge zero due to the protonation of phenolic and carboxylic acid groups. On the contrary, the fluorescein existed in an anionic form at pH 7.6 due to the ionization of functional groups, imparting a negative charge to the pore surface (Fig. 4A).

To evaluate the changes in rectification due to the ionization/deionization of the fluorescein, the *I–V* characteristics were recorded in slightly acidic and basic electrolyte solutions. Fig. 4B shows the *I–V* curves of the modified nanopore with "decaged" fluorescein moieties measured at pH 5.5 and pH 7.6. Under acidic conditions, the nanopore rectification was lost because of the neutral form of fluorescein: the nanopore behaved like an ohmic resistor, indicating an almost zero charge on the pore surface. On the contrary, under the basic conditions spirolactone ring-opening or ionization of functional groups led to the formation of anionic fluorescein which imparts a negative charge to the pore surface. This process resulted in the conversion of the nonselective pore to the cation permselective pore, leading to current rectification as seen in Fig. 4B. Thus, the slight pH change provides a feasible tool to externally tune the electrical characteristics of the nanopore by modulating the interactions between the charged surface and the mobile ionic species in solution under physiological conditions.

In addition to TBA$^+$ salts of halides, we have also checked the desilylation of "caged" fluorescein chains with sodium salts of fluoride (F^-), chloride (Cl^-), bromide (Br^-) and iodide (I^-) as well as other common anions such as sulphate (SO_4^{2-}), nitrate (NO_3^-), acetate (CH_3COO^-), bicarbonate (HCO_3^-) and hydrogen phosphate (HPO_4^-). Fig. 5A shows the *I–V* curves of another conical nanopore before and after the immobilization of "caged" fluorescein chains. Because of the neutral nature of the attached fluorescein moieties, the pore became nonselective (linear *I–V* behavior) after modification. To check the sen-

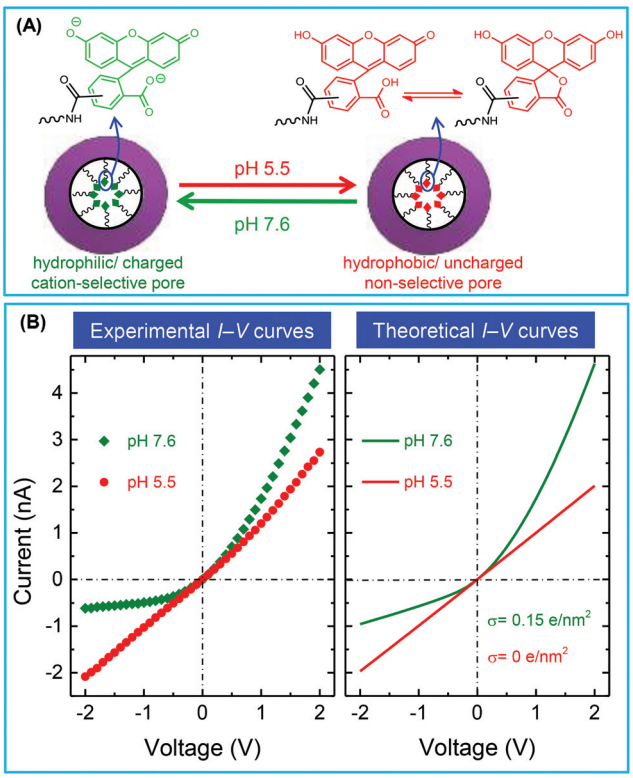

Fig. 4 (A) Scheme showing the pH-dependent changes in the structure of fluorescein. (B) *I–V* curves of the modified nanopore having "decaged" fluorescein moieties under acidic (pH 5.5) and basic (pH 7.6) conditions. The error bars of the experimental data are smaller than the symbol size.

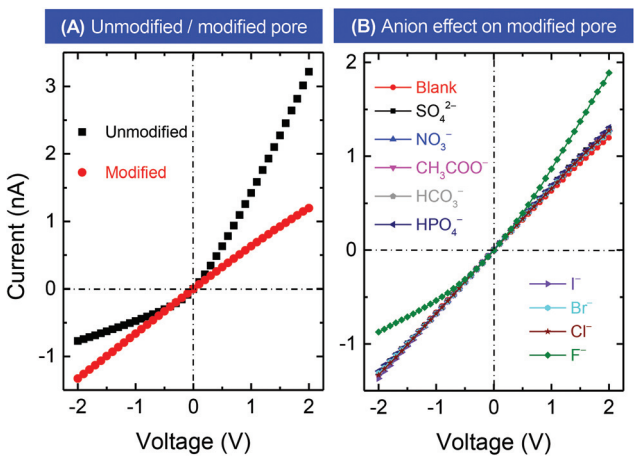

Fig. 5 (A) *I–V* characteristics of the single conical pore measured in 0.1 M KCl (pH 7.6) solution before (black) and after (red) the immobilization of "caged" fluorescein moieties. The radii of small and large pore openings are 8 and 280 nm, respectively. (B) *I–V* characteristics of the modified pore before (blank) and after the addition of 1 mM concentration of various anions (sodium salts) in the electrolyte solution separately. The error bars of the experimental data are smaller than the symbol size.

sitivity of the system, the *I–V* curves of the modified pore were recorded in the presence of various anions (sodium salts) in the electrolyte solution separately. From Fig. 5B, addition of Cl^-, Br^-, I^-, SO_4^{2-}, NO_3^-, CH_3COO^-, HCO_3^- and HPO_4^- in the electolyte solution did not cause any change in the *I–V* characteristics of the modified pore. On the contrary, exposure to the fluoride ion led to a significant change in *I–V* behavior: current rectification was observed due to the fluoride mediated hydrolysis of silyl ether and the concomitant emergence of negatively charged phenolate and carboxylate groups on the fluorescein moieties. These results confirmed further that the sensor exhibits excellent selectivity towards fluoride over other competitive anions.

From the *I–V* curves in Fig. 3 and 5, a clear difference in the capability of TBAF and NaF towards the selective removal of TBDPS moieties from the functionalized pore surface is observed. The Si–O bond cleavage depends on the availability of the fluoride anion. In the case of the TBAF salt, the counterion (TBA^+), *i.e.*, four bulky butyl groups on nitrogen (Bu_4N^+) makes the fluoride anion available for nucleophilic attack on the silicon atom. Moreover, the formation of the strong Si–F bond acted as a big driving force for the fast cleavage of TBDPS moieties from the pore surface. In the case of NaF, the highly attractive forces between the cations (Na^+) and anions (F^-) make the fluoride anion less available to attack the silicon atom. The value of f_{rec} is directly related to pore surface charge density. Therefore, in the cases of TBAF and NaF, the recovery of f_{rec} is ~91% and ~52%, respectively, compared to the corresponding unmodified pores. This fact clearly shows that the cleavage rate of TBDPS moieties and the generation of charged groups on the pore surface are higher for TBAF than for NaF.

Conclusions

Anions play a crucial role in chemical and biological processes and, in particular, fluoride is involved in cell signaling and transduction. Sensing devices that are functional only in organic solvents or mixed organic–water solutions have a limited use in biological applications. Other sensors based on ion channels inserted in lipid bilayers are not as robust as synthetic pores. We have designed a sensing nanodevice that selectively detects fluoride under physiological conditions.

In particular, we have demonstrated experimentally and theoretically a nanofluidic fluoride sensing device based on a single conical pore functionalized with "caged" fluorescein moieties. The nanopore functionalization is based on an amine-terminated fluorescein whose phenolic hydroxyl groups are protected with *tert*-butyldiphenylsilyl moieties. The protected fluorescein molecules are then immobilized on the nanopore surface *via* carbodiimide coupling chemistry. On exposure to fluoride anions, the asymmetrical distribution of charged groups along the conical nanopore leads to the electrical rectification observed in the *I–V* curve. On the contrary, other halides and anions are not able to induce any significant ionic rectification in the asymmetric pore. The theoretical results based on the Nernst–Planck and Poisson equations further confirm the validity of the experimental approach to fluoride-induced nanopore modulation.

Acknowledgements

M. A., S. N. and W. E. acknowledge the funding from the Hessen State Ministry of Higher Education, Research and the Arts, Germany, under the LOEWE project iNAPO. P. R. and J. C. acknowledge financial support by the Generalitat Valenciana (Program of Excellence Prometeo/GV/0069), the Spanish Ministry of Economic Affairs and Competitiveness (MAT2015-65011-P), and FEDER. I. A. and C. M. N. acknowledge the financial support through the Helmholtz programme BioInterfaces in Technology and Medicine. The authors are thankful to Prof. Salvador Mafé (Universitat de València, Spain) for fruitful discussion and to Prof. Christina Trautmann from GSI (Department of Material Research) for support with the heavy ion irradiation experiments.

Notes and references

1 (*a*) P. A. Gale, *Chem. Soc. Rev.*, 2010, **39**, 3746–3771; (*b*) H. N. Kim, Z. Guo, W. Zhu, J. Yoon and H. Tian, *Chem. Soc. Rev.*, 2011, **40**, 79–93; (*c*) Y. Zhou, J. F. Zhang and J. Yoon, *Chem. Rev.*, 2014, **114**, 5511–5571; (*d*) P. D. Beer and P. A. Gale, *Angew. Chem., Int. Ed.*, 2001, **40**, 486–516.

2 (*a*) C. D. Anuradha, S. Kanno and S. Hirano, *Arch. Toxicol.*, 2000, **74**, 226–230; (*b*) M. Refsnes, P. E. Schwarze, J. A. Holme and M. Laêg, *Hum. Exp. Toxicol.*, 2003, **22**, 111–123; (*c*) T.-J. Cheng, T.-M. Chen, C.-H. Chen and Y.-K. Lai, *J. Cell. Biochem.*, 1998, **69**, 221–231.

3 K. Kirk, in *Biochemistry of the Elemental Halogens and Inorganic Halides*, Springer, USA, 1991, vol. 9A+B, pp. 19–68.

4 (*a*) J. R. Farley, J. E. Wergedal and D. J. Baylink, *Science*, 1983, **222**, 330–332; (*b*) M. Cametti and K. Rissanen, *Chem. Commun.*, 2009, 2809–2829; (*c*) E. S. Orwoll, *Endocrinol. Metab. Clin.*, 1998, **27**, 349–367.

5 (*a*) S. Y. Kim, J. Park, M. Koh, S. B. Park and J.-I. Hong, *Chem. Commun.*, 2009, 4735–4737; (*b*) P. Singh, M. Barjatiya, S. Dhing, R. Bhatnagar, S. Kothari and V. Dhar, *Urol. Res.*, 2001, **29**, 238–244; (*c*) E. T. Everett, *J. Dent. Res.*, 2011, **90**, 552–560.

6 (*a*) H. Zhao, L. A. Leamer and F. P. Gabbai, *Dalton Trans.*, 2013, **42**, 8164–8178; (*b*) M. Sarkar, R. Yellampalli, B. Bhattacharya, R. Kanaparthi and A. Samanta, *J. Chem. Sci.*, 2007, **119**, 91–97.

7 (*a*) B. Hille, *Ionic channels of excitable membranes*, Sinauer Associates Inc., Sunderland, MA, 3rd edn, 2001; (*b*) V. M. Aguilella, C. Verdia-Baguena and A. Alcaraz, *Phys. Chem. Chem. Phys.*, 2014, **16**, 3881–3893.

8 (*a*) H. Bayley and P. S. Cremer, *Nature*, 2001, **413**, 226–230; (*b*) K. Healy, *Nanomedicine*, 2007, **2**, 459–481; (*c*) S. Howorka and Z. Siwy, *Chem. Soc. Rev.*, 2009, **38**, 2360–

2384; (*d*) J. J. Kasianowicz, E. Brandin, D. Branton and D. W. Deamer, *Proc. Natl. Acad. Sci. U. S. A.*, 1996, **93**, 13770–13773; (*e*) H.-Y. Wang, Y. Li, L.-X. Qin, A. Heyman, O. Shoseyov, I. Willner, Y.-T. Long and H. Tian, *Chem. Commun.*, 2013, **49**, 1741–1743.

9 (*a*) C. Dekker, *Nat. Nanotechnol.*, 2007, **2**, 209–215; (*b*) K. Healy, B. Schiedt and A. P. Morrison, *Nanomedicine*, 2007, **2**, 875–897; (*c*) X. Hou, W. Guo and L. Jiang, *Chem. Soc. Rev.*, 2011, **40**, 2385–2401; (*d*) X. Hou, H. C. Zhang and L. Jiang, *Angew. Chem., Int. Ed.*, 2012, **51**, 5296–5307; (*e*) Z. S. Siwy and S. Howorka, *Chem. Soc. Rev.*, 2010, **39**, 1115–1132.

10 (*a*) L. Wen, Y. Tian, J. Ma, J. Zhai and L. Jiang, *Phys. Chem. Chem. Phys.*, 2012, **14**, 4027–4042; (*b*) H. Zhang, Y. Tian and L. Jiang, *Chem. Commun.*, 2013, **49**, 10048–10063; (*c*) M. Ali, S. Nasir, I. Ahmed, L. Fruk and W. Ensinger, *Chem. Commun.*, 2013, **49**, 8770–8772; (*d*) M. Ali, S. Nasir, P. Ramirez, I. Ahmed, Q. H. Nguyen, L. Fruk, S. Mafe and W. Ensinger, *Adv. Funct. Mater.*, 2012, **22**, 390–396; (*e*) M. Ali, S. Nasir, P. Ramirez, J. Cervera, S. Mafe and W. Ensinger, *ACS Nano*, 2012, **6**, 9247–9257; (*f*) M. Ali, P. Ramirez, S. Mafe, R. Neumann and W. Ensinger, *ACS Nano*, 2009, **3**, 603–608; (*g*) M. Ali, P. Ramirez, H. Q. Nguyen, S. Nasir, J. Cervera, S. Mafe and W. Ensinger, *ACS Nano*, 2012, **6**, 3631–3640; (*h*) S. Nasir, M. Ali and W. Ensinger, *Nanotechnology*, 2012, **23**, 225502; (*i*) S. Nasir, M. Ali, P. Ramirez, V. Gómez, B. Oschmann, F. Muench, M. Nawaz Tahir, R. Zentel, S. Mafe and W. Ensinger, *ACS Appl. Mater. Interfaces*, 2014, **6**, 12486–12494; (*j*) S. Nasir, P. Ramirez, M. Ali, I. Ahmed, L. Fruk, S. Mafe and W. Ensinger, *J. Chem. Phys.*, 2013, **138**, 034709; (*k*) Z. Siwy, E. Heins, C. C. Harrell, P. Kohli and C. R. Martin, *J. Am. Chem. Soc.*, 2004, **126**, 10850–10851; (*l*) H. Zhang, X. Hou, L. Zeng, F. Yang, L. Li, D. Yan, Y. Tian and L. Jiang, *J. Am. Chem. Soc.*, 2013, **135**, 16102–16110; (*m*) R. E. Gyurcsanyi, *TrAC, Trends Anal. Chem.*, 2008, **27**, 627–639; (*n*) M. Wanunu and A. Meller, *Nano Lett.*, 2007, **7**, 1580–1585.

11 (*a*) M. Ali, S. Nasir, Q. H. Nguyen, J. K. Sahoo, M. N. Tahir, W. Tremel and W. Ensinger, *J. Am. Chem. Soc.*, 2011, **133**, 17307–17314; (*b*) M. Ali, S. Nasir, P. Ramirez, J. Cervera, S. Mafe and W. Ensinger, *J. Phys. Chem. C*, 2013, **117**, 18234–18242; (*c*) M. Ali, R. Neumann and W. Ensinger, *ACS Nano*, 2010, **4**, 7267–7274; (*d*) M. Ali, P. Ramirez, M. N. Tahir, S. Mafe, Z. Siwy, R. Neumann, W. Tremel and W. Ensinger, *Nanoscale*, 2011, **3**, 1894–1903; (*e*) M. Ali, B. Schiedt, R. Neumann and W. Ensinger, *Macromol. Biosci.*, 2010, **10**, 28–32; (*f*) M. Ali, M. N. Tahir, Z. Siwy, R. Neumann, W. Tremel and W. Ensinger, *Anal. Chem.*, 2011, **83**, 1673–1680; (*g*) C. Han, H. Su, Z. Sun, L. Wen, D. Tian, K. Xu, J. Hu, A. Wang, H. Li and L. Jiang, *Chem. – Eur. J.*, 2013, **19**, 9388–9395; (*h*) X. Hou and L. Jiang, *ACS Nano*, 2009, **3**, 3339–3342; (*i*) Q. H. Nguyen, M. Ali, R. Neumann and W. Ensinger, *Sens. Actuators, B*, 2012, **162**, 216–222; (*j*) Z. Siwy, L. Trofin, P. Kohli, L. A. Baker, C. Trautmann and C. R. Martin, *J. Am. Chem. Soc.*, 2005, **127**, 5000–5001; (*k*) Y. Tian, X. Hou, L. P. Wen, W. Guo, Y. L. Song, H. Z. Sun, Y. G. Wang, L. Jiang and D. B. Zhu, *Chem. Commun.*, 2010, **46**, 1682–1684; (*l*) I. Vlassiouk, T. R. Kozel and Z. S. Siwy, *J. Am. Chem. Soc.*, 2009, **131**, 8211–8220.

12 P. Y. Apel, Y. E. Korchev, Z. Siwy, R. Spohr and M. Yoshida, *Nucl. Instrum. Methods Phys. Res., Sect. B*, 2001, **184**, 337–346.

13 J. Brglez, I. Ahmed and C. M. Niemeyer, *Org. Biomol. Chem.*, 2015, **13**, 5102–5104.

14 R. Appiah-Ntiamoah, W.-J. Chung and H. Kim, *New J. Chem.*, 2015, **39**, 5570–5579.

15 (*a*) J. Cervera, P. Ramirez, S. Mafe and P. Stroeve, *Electrochim. Acta*, 2011, **56**, 4504–4511; (*b*) J. Cervera, B. Schiedt, R. Neumann, S. Mafe and P. Ramirez, *J. Chem. Phys.*, 2006, **124**, 104706; (*c*) J. Cervera, B. Schiedt and P. Ramirez, *Europhys. Lett.*, 2005, **71**, 35–41; (*d*) P. Ramirez, P. Y. Apel, J. Cervera and S. Mafe, *Nanotechnology*, 2008, **19**, 315707; (*e*) P. Ramirez, V. Gomez, J. Cervera, B. Schiedt and S. Mafe, *J. Chem. Phys.*, 2007, **126**, 194703; (*f*) Z. Siwy and A. Fulinski, *Am. J. Phys.*, 2004, **72**, 567–574; (*g*) Z. S. Siwy, *Adv. Funct. Mater.*, 2006, **16**, 735–746.

16 (*a*) R. Chavali, N. S. K. Gunda, S. Naicker and S. K. Mitra, *Anal. Chem. Res.*, 2015, **6**, 26–31; (*b*) J. Cao, C. Zhao and W. Zhu, *Tetrahedron Lett.*, 2012, **53**, 2107–2110; (*c*) R. Hu, J. Feng, D. Hu, S. Wang, S. Li, Y. Li and G. Yang, *Angew. Chem., Int. Ed.*, 2010, **49**, 4915–4918; (*d*) G. Wei, J. Yin, X. Ma, S. Yu, D. Wei and Y. Du, *Anal. Chim. Acta*, 2011, **703**, 219–225.

17 (*a*) V. Zanker and W. Peter, *Chem. Ber.*, 1958, **91**, 572–580; (*b*) H. Leonhardt, L. Gordon and R. Livingston, *J. Phys. Chem.*, 1971, **75**, 245–249; (*c*) M. M. Martin and L. Lindqvist, *J. Lumin.*, 1975, **10**, 381–390.